CrossMark

Nanostructures confined self-assembled in biomimetic nanochannels for enhancing the sensitivity of biological molecules response

Qiao Chen[1] · Yongqian Wang[1] · Mingyan Zheng[2] · Hao Fang[1] · Xiang Meng[1]

Abstract

The combination of biomimetic nanochannels and nanostructures provided a new idea for bioanalytical purposes. In this paper, we reported a self-assembled system based on the integration of anodic aluminum oxide (AAO) membranes and CuO method to fabricate CuO nanostructures in the confined area of AAO membranes. Furthermore, we investigated morphologies of the self-assembly systems by field emission scanning electron microscopy (FESEM) and characterized the type and content of microelements by energy dispersive spectrometer. Transmembrane ion current through nanochannels was tested by an electrochemical workstation, and optical properties of the self-assembly systems were characterized by ultraviolet–visible spectrophotometer. We could conclude from the results that the morphology and distribution status of CuO nanostructures are controllable, while ionic current through nanochannels and optical properties of self-assembled systems could be regulated by changing experimental parameters such as electrodeposition time, electrodeposition voltage or annealing temperature. On this base, we utilized the synergistic effect of nanochannels and nanostructures to enhance the sensitivity of biological molecules response. This study not only prepared CuO nanostructures in biomimetic nanochannels controllably, but also provided a novel application paradigm for nanochannels-nanostructures self-assembled system, which could be used for biological analysis and detection.

1 Introduction

In recent years, nanostructures of transition metal oxides have attracted wide attention because of their superior properties compared with the corresponding bulk counterparts, and have promising application prospects in various fields of technology [1–5]. As one of the most popular transition metal oxide, copper oxide (CuO) is a *p* type semiconductor with a narrow band gap of 1.2 eV [6, 7]. It possesses monoclinic structure and many unique characteristics, for example, superior catalytic activity, super thermal conductivity,

photovoltaic properties, and high stability [1–3]. Due to such exclusive properties, CuO can be applied to many science fields: active catalyst [2], high T_C superconductors [8], high efficiency thermal conducting material [9], magnetic storage media [10], solar cell [11], gas sensor [12], nonenzymatic glucose sensing [13], and so on. The unique physical and chemical properties of CuO nanostructures strongly rely on its morphology, size, specific surface area and preparation methods [14]. Therefore, it is necessary to prepare CuO nanostructures with high quality, controllable size and morphology in a confined area. Inspired by ion channels in living bodies, scientists have begun research on artificial biomimetic nanochannels. Biomimetic nanochannels can be conducted various symmetric and asymmetrical modifications to gain bionic intelligence performance [15]. In the case, AAO is one of the most popular inorganic materials to produce nanochannels due to its controllable pore-diameter, depth, shape, and periodic pattern [16]. In addition, the stable chemical property and single surface group are propitious to decorate different materials with nanostructures on the surface or channel inner wall of AAO membrane, which in turn changes the physical and chemical properties of nanochannels [17, 18].

✉ Yongqian Wang
cugwyq@126.com

✉ Mingyan Zheng
zhengmy@cug.edu.cn

1 Engineering Research Center of Nano-Geomaterials of Ministry of Education, Faculty of Materials Science and Chemistry, China University of Geosciences, 388# Lumo Road, Wuhan 430074, People's Republic of China

2 Faculty of Engineering, China University of Geosciences, 388# Lumo Road, Wuhan 430074, People's Republic of China

Some researchers have reported that CuO nanostructures were assembled in biomimetic nanochannels by different methods. Chueh's group synthesized large-scale nanotwinned Cu nanowire arrays from anodic aluminum oxide membrane by electrochemical deposition process, furthermore investigated its different growth orientations of nanotwinned Cu nanowire arrays and electrical endurance performance [19]. Yang's group fabricated oriented copper oxide nanowire arrays by a general melt-injection-decomposition route within AAO membrane [20]. Gao's group synthesized highly ordered CuO nanowire arrays of composite-oxides within AAO template by a citrate-based sol–gel route [21]. Ramesh's group deposited bare SnO_2 and SnO_2/CuO bilayer thin films directly on AAO template by pulsed laser deposition and then used them as a gas sensor without additional processing [22].

Most researchers have only studied the performance of CuO nanostructures alone by dissolving AAO with aqueous solution of acid or alkali, but few of them have considered AAO membranes and CuO nanostructures as a whole [19–22]. Hence, we not only prepared CuO nanostructures in biomimetic nanochannels by electrochemical deposition process controllably, but also studied the overall performance of AAO membrane and CuO nanostructures. In addition, we used the synergistic effect of nanochannels and nanostructures to improve the sensitivity of biological molecules response [23–25].

2 Experimental

2.1 Materials

All reagents in this experiment were of analytical grade and used without further purification. Deionized water was used for the preparation for all solution. AAO membranes with a diameter of about 80–100 nm and a thickness of about 60 ± 5 μm were purchased from Pu-Yuan Nano Technology Co. Ltd (Hefei, China). Cupric nitrate ($Cu(NO_3)_2 \cdot 3H_2O$) and potassium chloride (KCl) were supplied from Sinopharm Chemical Reagent Co. Ltd (Beijing, China). L-Cysteine was purchased from Sinopharm Chemical Reagent Co. Ltd (Beijing, China). D-Cysteine was purchased from Macklin. Bovine serum albumin (BSA) was purchased from BioFroxx.

2.2 Experimental procedure

2.2.1 CuO nanostructures confined self-assembled

Anodic aluminum oxide (AAO) template with diameter of 80–100 nm was used as carriers and tailored into square shape with dimensions of 1 cm × 2 cm, which should be

coated with gold with thickness of 20 nm by vacuum coating instrument to make it conductive. The electrolyte contains copper nitrate ($Cu(NO_3)_2 \cdot 3H_2O$, 0.1 M) and potassium chloride (KCl, 0.1 M) mixture aqueous solution with an amount of 35–40 ml. Saturated calomel electrode was used as reference electrode, platinum electrode served as anode and a AAO membrane fixed on the PTFE electrode clamp was acted as cathode, in this electrochemical deposition process. The electrode was fixed in an electrolytic cell, and the electrolyte was poured thereinto. The cell was then placed in a constant temperature water bath to maintain the electrolyte temperature at 70 °C. The schematic diagram of electrochemical deposition process is shown in Scheme 1a. The electrochemical deposition process was conducted with proper voltage and time. Finally, the obtained samples were put into a muffle for 2 h.

2.2.2 L-Cys/D-Cys was decorated in AAO nanochannels

We modified L-Cys or D-Cys in the AAO channels by solution impregnation with the help of UV light. First, we prepared a certain amount of 10 mM L-Cys solution and 10 mM D-Cys solution. Then we put the AAO templates decorated with CuO nanostructures and the L-Cys solution (10 mM)
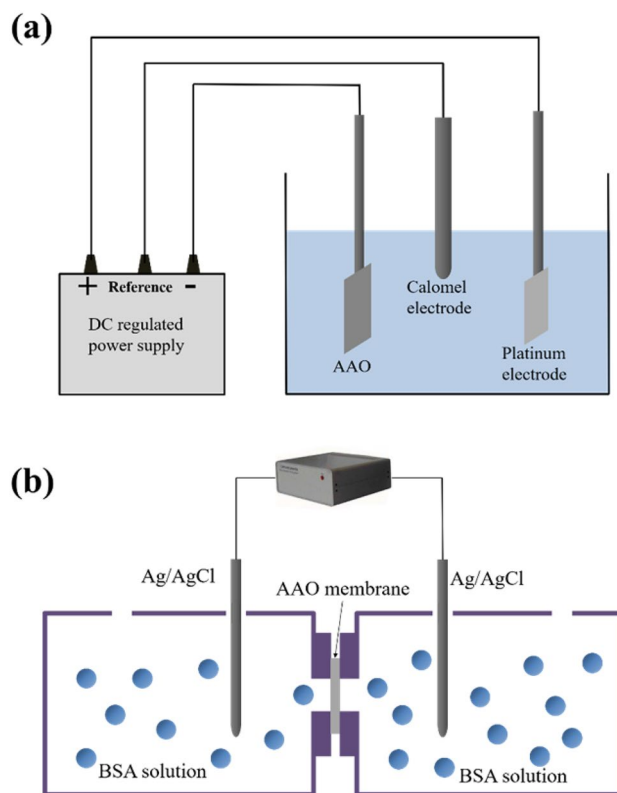

Scheme 1 **a** Schematic diagram of electrochemical deposition device. **b** The experimental device diagram of the BSA transport experiment

Fig. 1 The FESEM images of **a** unannealed samples, **b** annealed samples. (The insert maps showed the surface topography of the samples.)
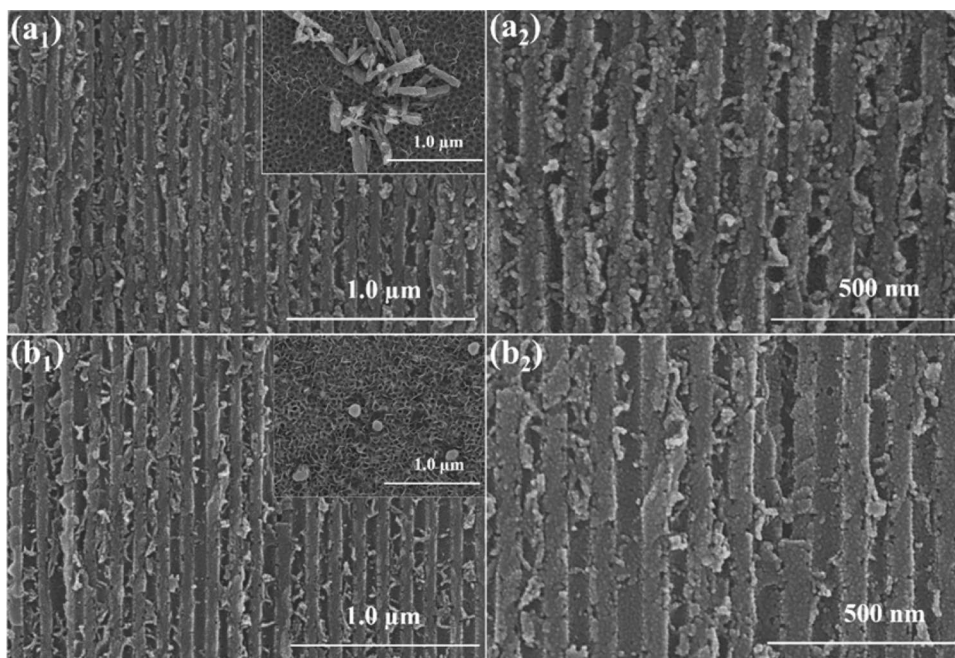
Scheme 2 Schematic diagram of the fabrication processes of nanochannels-nanostructures self-assembly system
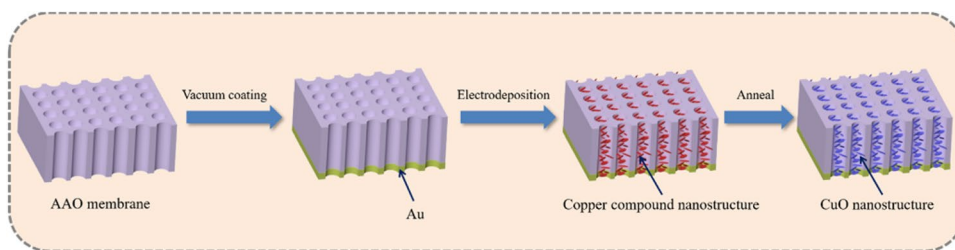
Fig. 2 **a** UV–Vis transmissivity of bare AAO, annealed and unannealed samples. **b** I–V curves of bare AAO channels, annealed and unannealed samples. (All the electrolyte were 0.1 M KCl, pH value was 7.0.)
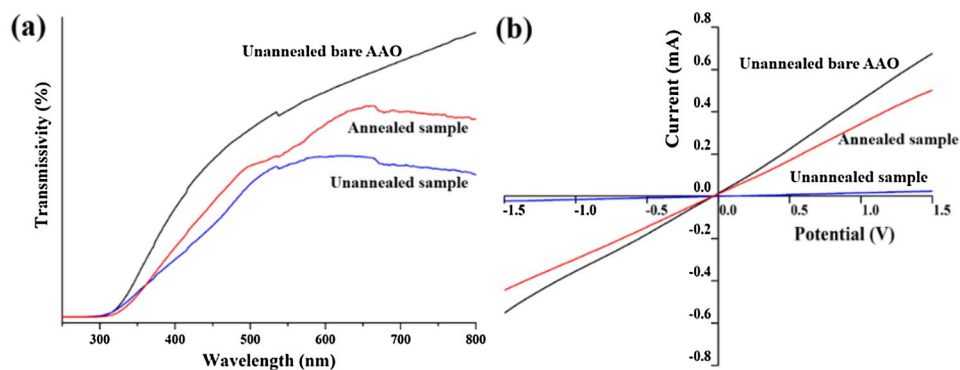

or D-Cys solution (10 mM) into the 10 ml centrifuge tube. Finally, the centrifuge tubes were exposed to UV light (365 nm) overnight.

2.3 Characterization

The morphology of samples was characterized by a field emission scanning electron microscopy (FESEM, Hitachi SU-8010). The microelements analysis was conducted by energy dispersive X-ray spectroscopy (EDS, that is fitted to the Hitachi SU-8010 FESEM). Electrochemical station (CHI 660E) was used to test the transmembrane ion current of nanochannels, by using a self-made two-electrode cell in a buffer solution (pH value is 7.0, 0.1 M KCl), and the symmetric Ag/AgCl electrodes as working and counter electrode. Transmissivity of samples were characterized by

Fig. 3 The FESEM images of samples prepared by different electrodeposition time: **a** 10 min, **b** 20 min, **c** 30 min, **d** 40 min, **e** 50 min. (The insert maps showed the surface topography of the samples.)
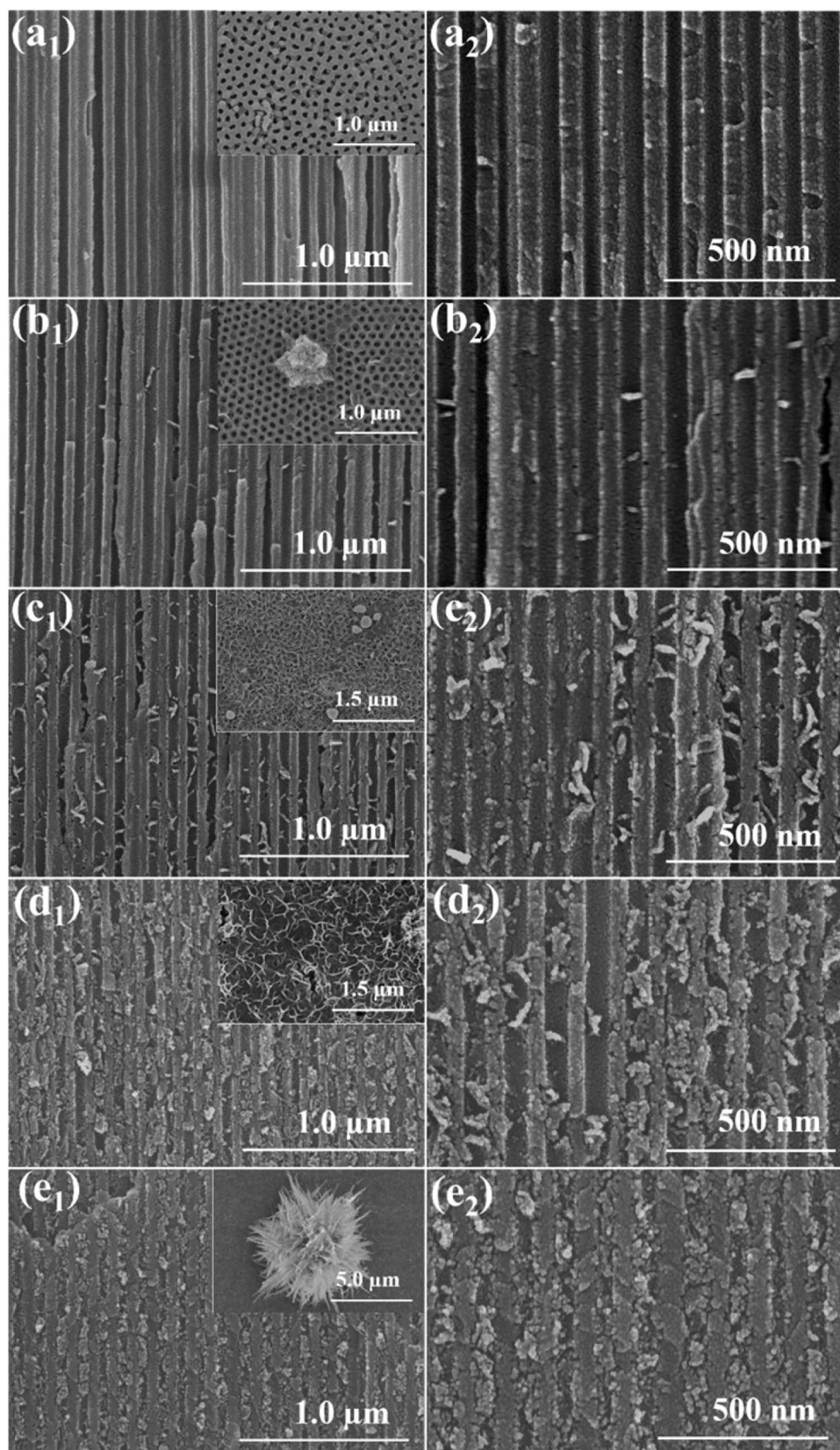
Fig. 4 **a** UV–Vis transmission spectra of samples prepared under different electrodeposition time. **b** The value of transmissivity of samples prepared under different electrodeposition time at 660 nm. **c** I–V curves of samples prepared under different electrodeposition time. (All the electrolyte were 0.1 M KCl, pH value was 7.0.)
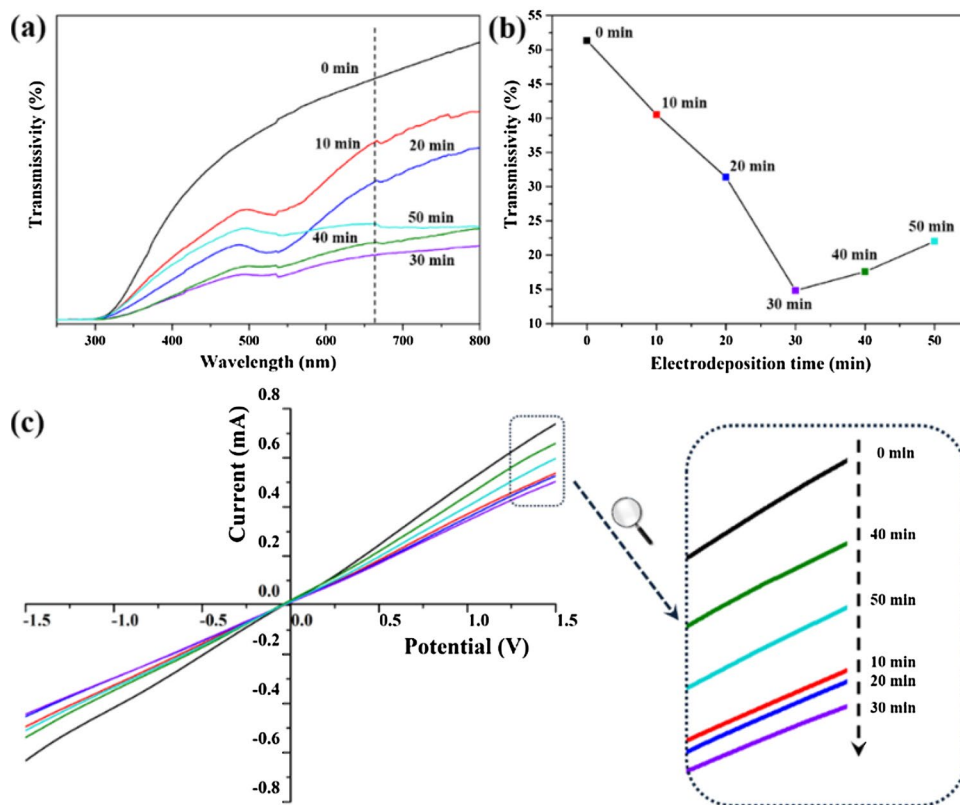
ultraviolet–visible (UV–Vis) spectrophotometer (Shimadzu UV-2550). The surface plane of AAO membrane was placed in a vertical position relative to the UV/Vis light path with the help of membrane rack accessories. The transmission spectra of the membranes were measured in the wavelength range from 800 to 250 nm.

3 Results and discussion

3.1 Influence of annealing

The surface and section morphologies of unannealed and annealed samples were analyzed by FESEM and results were shown in Fig. 1. We could obviously observe that nanostructures were anchored to the inner wall of both unannealed and annealed samples. The nanostructures in the nanochannels of unannealed samples were incompact and had no fixed shape (Fig. 1a). Cube-like block structures could be observed on the surface of unannealed samples. After annealing, flaky CuO nanostructures with similar shape was evenly grown in AAO nanochannels, and spherical shape nanostructures were fabricated on the surface of samples (Fig. 1b). This phenomenon is caused by annealing to remove the crystalline water of the nanostructure, changing its grain size and lattice parameters. The schematics of the fabrication processes of

nanochannels-nanostructures self-assembly system were shown in Scheme 2.

Figure 2a showed the UV–Vis transmission spectra of unannealed and annealed samples. In general, when the wavelength was less than 300 nm, transmissivity of the samples were relatively low, and grew steadily as the wavelength was from 300 to 660 nm, then decreased slowly until 800 nm. The transmission rate of the annealed sample was bigger than the unannealed sample, except for 300–350 nm. In a sense, the assembly density of CuO nanostructures could be reflected by the transmittance. The nanostructures assembly density of the unannealed samples were larger than the annealed samples according to the transmission spectra.

As shown in the Fig. 2b, we could see that the ionic current declined obviously when AAO membranes was assembled with nanostructures. After annealing, the ionic current of the sample increased, but it was still less than the ionic current of the bare AAO. The nanostructures would hinder the migration of ions in the nanochannels, resulting in a decrease in transmembrane ion currents. Annealing would make the assembly density of the nanostructures smaller, thereby increasing the ionic current. This was consistent with the result of transmission spectra. It was not easy to analyze the ingredients of unannealed samples, and it could be oxidized to cause erratic performance. Therefore, we mainly studied the performance of annealed samples.

Fig. 5 The FESEM images of samples prepared by different electrodeposition voltage: **a** 0.1 V, **b** 0.5 V, **c** 1.0 V, **d** 1.5 V, **e** 2.0 V. (The insert maps showed the surface topography of the samples.)
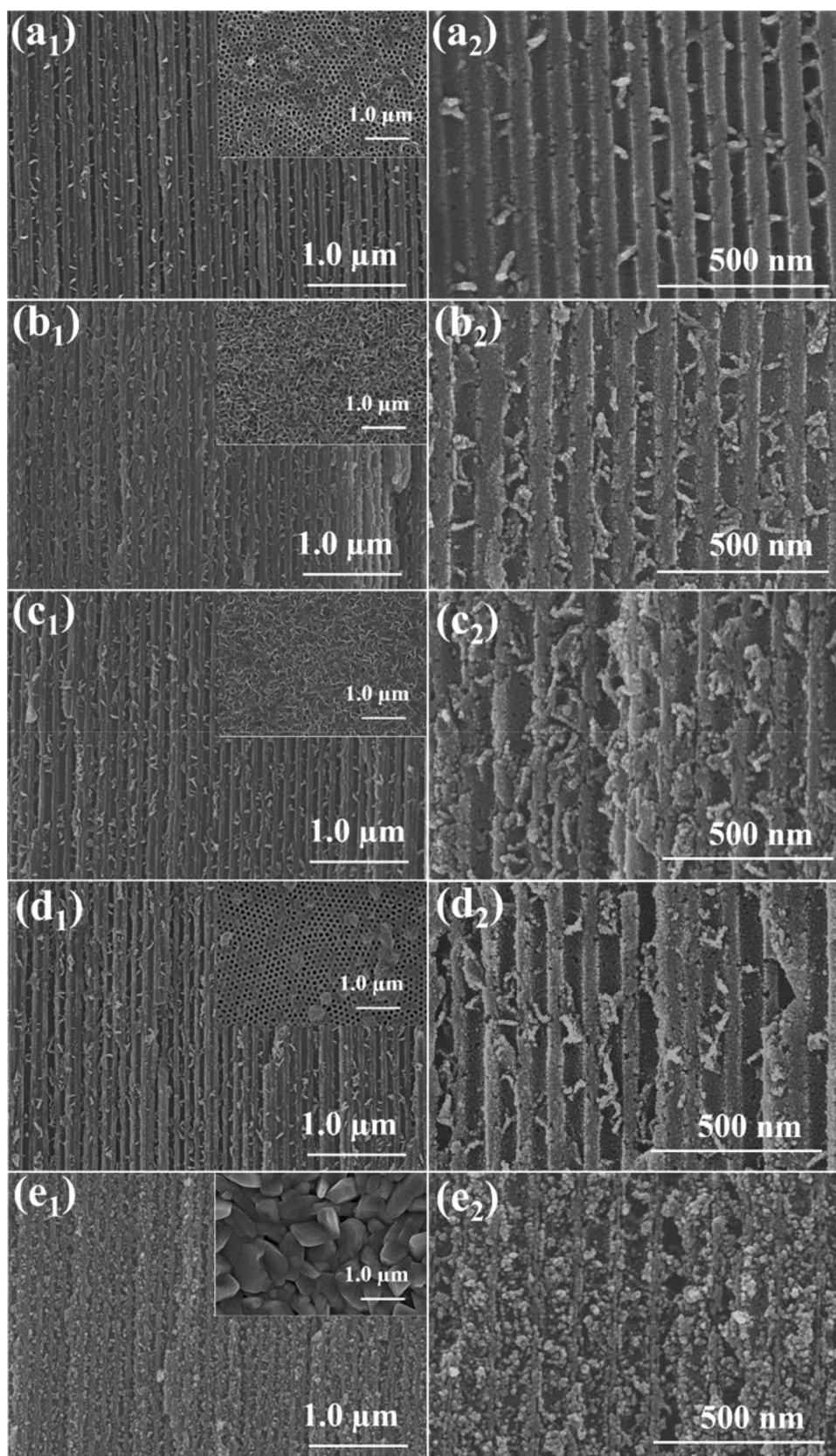
Fig. 6 **a** UV–Vis transmission spectra of samples prepared under different electrodeposition voltage. **b** The value of transmissivity of samples prepared under different electrodeposition voltage at 660 nm. **c** I–V curves of samples prepared under different electrodeposition voltage. (All the electrolyte were 0.1 M KCl, pH value was 7.0.)
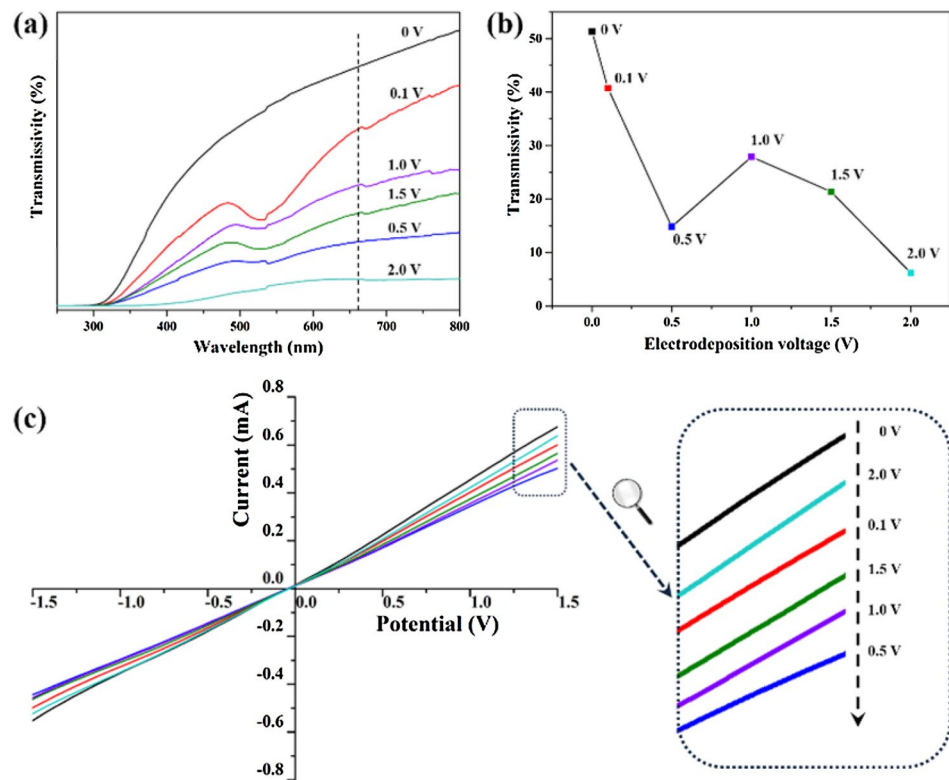
3.2 Influence of electrodeposition time

Figure 3 showed a FESEM image of samples prepared by different electrodeposition time. With the increase of the deposition time, the morphology of the inner wall and surface of AAO membranes significantly changed. As shown in the Fig. 3a, CuO nanostructures were hardly observed on the inner wall or surface of the samples at electrodeposition time of 10 min. Figure 3b showed that a small amount of bare CuO nanostructures were found on the inner wall of the samples at electrodeposition time of 20 min, and flower-like nanostructures appeared on the surface of AAO membranes. When the electrodeposition time increased to 30 min, lamellar CuO nanostructures grew in the channels of AAO membranes, and spherical shape nanostructures grew from the previous flower-like crystals (Fig. 3c). Figure 3d, e showed that more CuO nanostructures in the channels of AAO membrane were gathered together to form homogeneous clusters, and the morphology of the sample surface also changed, with the increase of the deposition time. In general, the assembly density of CuO nanostructures in the pore was proportional to the electrodeposition time.

Figure 4a showed the UV–Vis transmission spectra of samples with different electrodeposition time. The change trend of transmissivity is basically the same as that of the previous samples. Figure 4b showed the value of transmissivity of samples prepared under different electrodeposition

time at 660 nm. We could conclude that the transmittance of the samples decreased firstly with increasing electrodeposition time and then increased. When the electrodeposition time was 30 min, the value of transmissivity of the sample was the minimum. Figure 4c showed I–V curves of samples prepared under different electrodeposition time. The ironic current of nanochannels decorated with CuO nanostructures was smaller than bare AAO membranes, which indicated that CuO nanostructures in the AAO channels hindered the transfer of ions. When electrodeposition time was 30 min, the ionic current was minimal. The assembly density of CuO nanostructures in the inner wall of AAO membranes would affect the transmembrane ionic current and UV–Vis transmissivity of samples, but that was not the only factor. The change of AAO membranes pore size caused by annealing and different surface nanostructures would also influence its properties. To sum up, we hold the view that the best condition is when the electrodeposition time is 30 min.

3.3 Influence of electrodeposition voltage

Figure 5 showed FESEM images of samples prepared by different electrodeposition time. The CuO nanostructures in the nanochannels of different samples were approximately the same lamellar structure, but the distribution density was different, which was observed from Fig. 5a–e. When the electrodeposition voltage reached 2V, the CuO nanostructures

Fig. 7 The FESEM images of samples prepared by different annealing temperature: **a** 300 °C, **b** 350 °C, **c** 400 °C, **d** 450 °C, **e** 500 °C. (The insert maps showed the surface topography of the samples.)
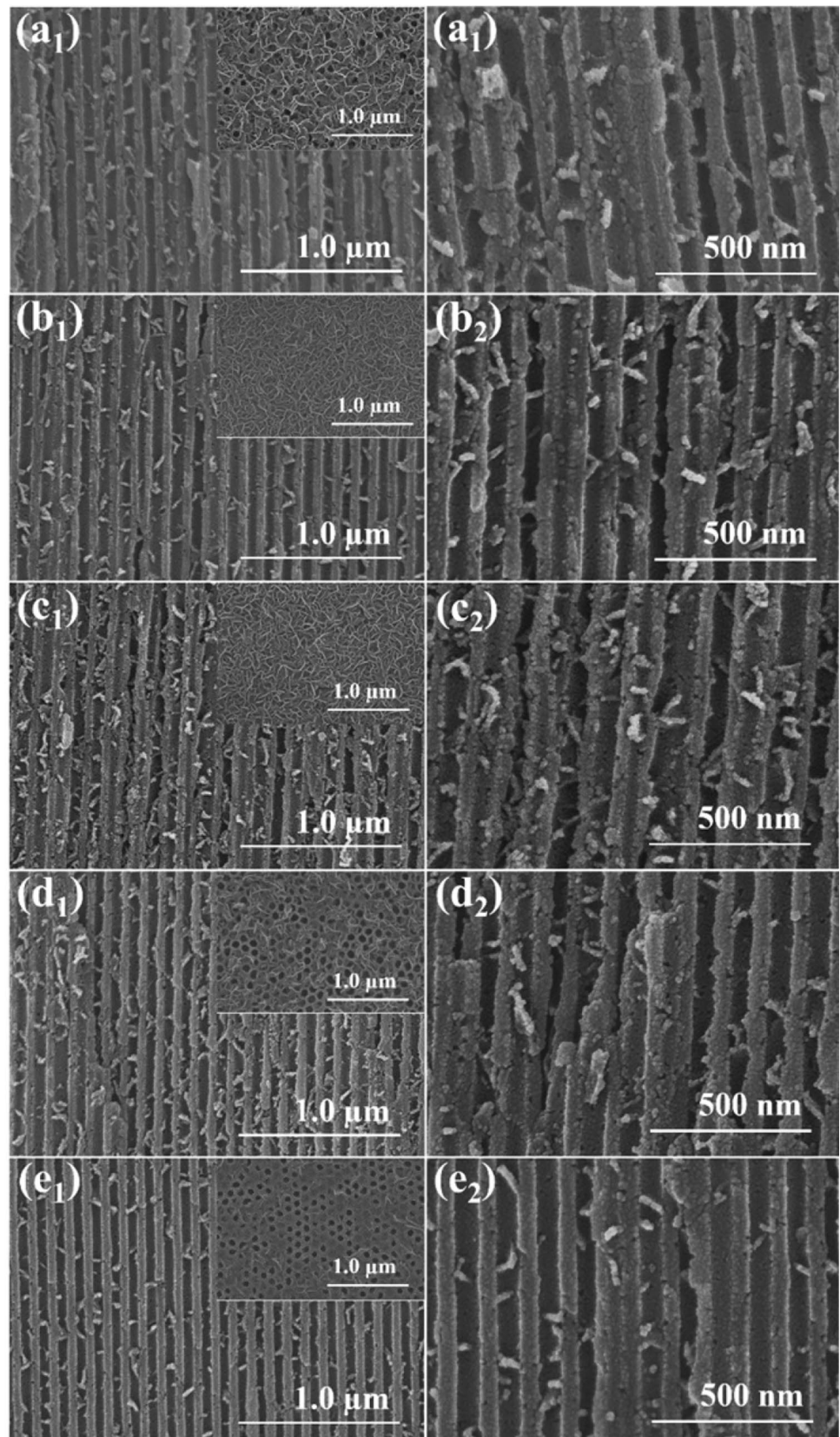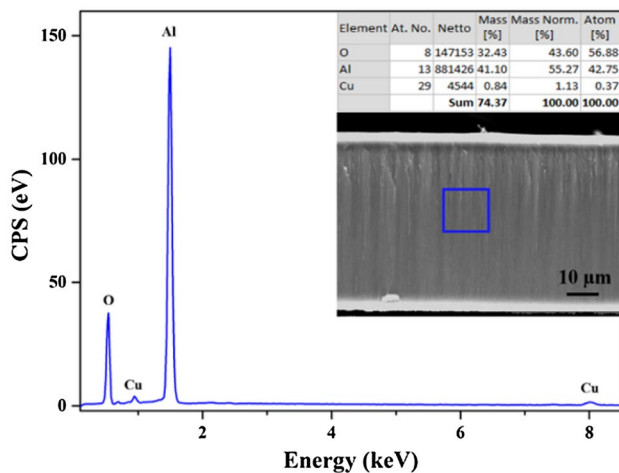
Fig. 8 EDS spectrum of the sample prepared at 400 °C annealing temperature

had a high assembly density. As illustrated in the insert maps of Fig. 5a–e, a layer of moss-like nanostructures grew on the surface of the samples. As the electrodeposition voltage increased, the nanostructures would become denser and eventually formed dense polygonal crystals.

Figure 6a, b showed that the UV–Vis transmission spectra and the value of transmissivity at 660 nm of samples with different electrodeposition voltage respectively. When the electrodeposition voltage was 2 V, the value of transmissivity of the sample was the smallest, because the copper oxide had the highest assembly density at this time. Figure 6c showed I–V curves of samples prepared under different electrodeposition voltage. When the electrodeposition voltage was 2 V, the ion current of the sample was minimum.

We could see that the transmembrane ion currents of the samples are relatively high at the electrodeposition voltage of 2 V. This may relate to the destruction of nanochannels. From the above experimental results, we could recognize that the CuO nanostructures assembly was the best when the electrodeposition voltage was 0.5 V.

### 3.4 Influence of annealing temperature

As shown in the Fig. 7a–e, the lamellar CuO nanostructures were found in the nanochannels of different samples prepared by different annealing temperature, and the growth density of nano-structure increased first and then decreased with the increased of annealing temperature. When annealing temperature was 400 °C, the CuO nanostructures had the best assembly effect (Fig. 7c). The insertion diagrams of Fig. 7a–e showed the moss-like nanostructure growing on the surface of the samples under all annealing conditions.

To explore the type and content of microelements in materials, energy-dispersive X-ray spectroscopy (EDS) analysis was used for this characterization. Figure 8 shows the EDS mapping results of the sample prepared under 400 °C. From the chart, we could see that the composition of copper is 1.13%, oxygen and aluminum is 43.6% and 55.27% respectively. Oxygen and aluminum elements were mainly derived from AAO membranes. Combined with the EDS results and annealing process, we could judge the composition of the nanostructures as copper oxide.

3.5 Application of biological molecules response

Protein transport is an important process of life and is strongly influenced by chiral interaction [23–25]. Based on

Scheme 3 The mechanism diagram of the BSA transport experiments
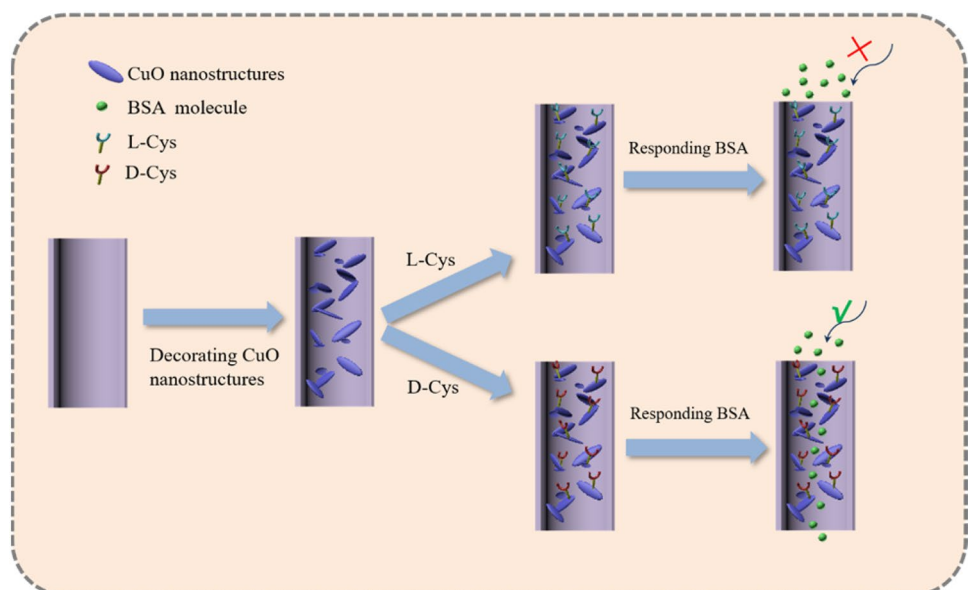
Fig. 9 **a** I–V curves of BSA transport after AAO channels modified by L-Cys/D-Cys. **b** I–V curves of BSA transport after AAO channels modified by L-Cys and AAO channels decorated with CuO nanostructures and modified by L-Cys. **c** I–V curves of BSA transport after AAO channels modified by D-Cys and AAO channels decorated with CuO nanostructures and modified by D-Cys. **d** I–V curves of BSA transport after AAO channels decorated with CuO nanostructures and modified by L-Cys/D-Cys. **e** The ionic current change ratio of BSA transport after AAO channels decorated with CuO nanostructures and modified by L-/D-Cys at different BSA concentration. (All the BSA were dissolved in 0.1 M KCl, pH value was 7.0.)
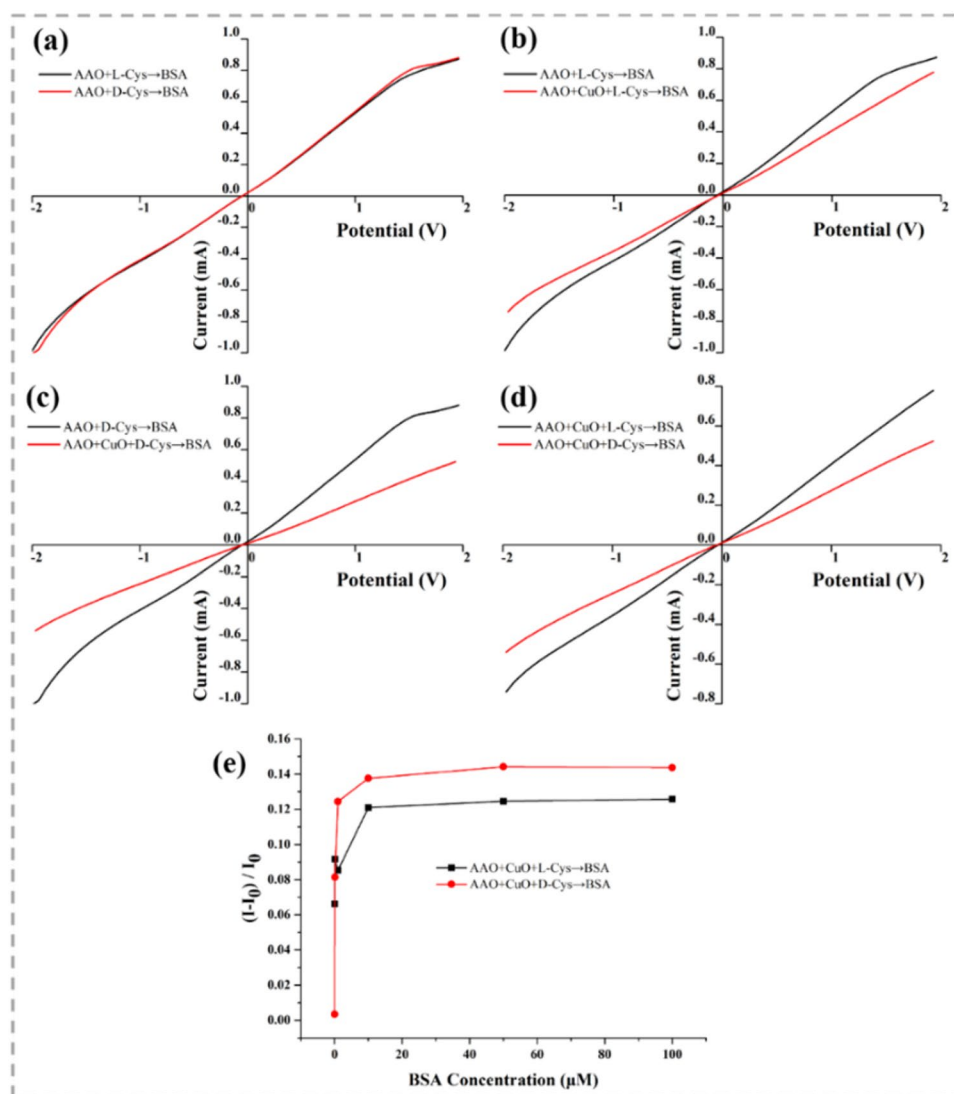
the selective permeability of artificial biomimetic nanochannels and large specific surface area of nanostructures, we designed nanochannels decorated nanostructures and modified chiral amino acids to enhance the sensitivity of biological molecules response. The experimental device diagram of the transport experiment was shown in scheme 1b. We modified the L-Cys/D-Cys into the nanochannels of pre-prepared self-assembly systems by impregnation method and selected BSA as the protein transport model. The value of transmembrane ion currents was used to characterize the differences in the response of biomolecules. The mechanism diagram of the BSA transport experiments was shown in scheme 3. L-Cys/D-Cys were modified on the inner wall of AAO by van der Waals force. The Cys enantiomers modified chiral nanopores are positively charged, but BSA is slight negatively charged. The mechanism of chirality facilitated protein translocation can be proposed as a two-step process: Firstly, chiral selectivity interaction facilitated the protein enter into

the nanopore and transient gathering on the nanopores surface. Secondly, under the electric field driven, the protein leaves off the surface and translocation [24, 25].

We modified L-Cys or D-Cys in the AAO channels, and then used 10 μM BSA for the transport experiments. As shown in the Fig. 9a, when L-Cys and D-Cys respectively modified the AAO channel, the I–V curves of BSA transport were almost identical. Compared with the AAO channels modified by L-Cys, the ionic currents of AAO channels decorated with CuO nanostructures and modified by L-Cys decreased slightly (Fig. 9b). From Fig. 9c we could see that the ionic current of AAO channels decorated with CuO nanostructures and modified by D-Cys had a marked decrease, compared with the AAO channels modified by D-Cys. Figure 9d showed the I–V curves of BSA transport after AAO channels decorated with CuO nanostructures and modified by L-Cys/D-Cys respectively. There was a big difference in transmembrane ion currents caused by

L-Cys/D-Cys response to BSA, which indicates that our pre-prepared AAO channels-CuO nanostructures self-assembly systems can be applied for enhancing the sensitivity of biological molecules response. Furthermore, we used different concentration BSA for the transport experiments. Figure 9e showed that the change rate of the current increased significantly, when the BSA concentration increased from 0.001 to 10 M, and then the current change rate tended to stabilize as the increased of BSA concentration. This illustrated that the best concentration range for BSA transport experiments was 10–100 μM.

4 Conclusions

In summary, we prepared CuO nanostructures in AAO nanochannels by electrochemical deposition process controllably, and discussed the effect of experimental parameters on the performance of the self-assembled systems. The morphology and assembly density of CuO nanostructures, ionic current through nanochannels and transmission of self-assembled systems could be regulated by adopting different experimental conditions such as electrodeposition time, electrodeposition voltage or annealing temperature. On this basis, we used the pre-prepared self-assembled systems to respond to BSA molecules by modifying L-Cys and D-Cys respectively. Experimental results show that the sensitivity of biological molecules response can be improved by assembling the CuO nanostructures in the AAO nanochannels. This work envision the new perspective of nanochannels-nanostructures could pave the way for high-sensitivity biological analysis and detection.

References

1. T.T. Ha, N.V. Tuyen, Copper oxide nanomaterials prepared by solution methods, some properties, and potential applications: a brief review. Int. Sch. Res. Not. **2014**(13), 1–14 (2014)

2. Y. Yecheskel, I. Dror, B. Berkowitz, Catalytic degradation of brominated flame retardants by copper oxide nanoparticles. Chemosphere **93**(1), 172–177 (2013)

3. Q. Zhang, K. Zhang, D. Xu et al., CuO nanostructures: synthesis, characterization, growth mechanisms, fundamental properties, and applications. Prog. Mater. Sci. **60**(1), 208–337 (2014)

4. Y. Wang, D. Wang, B. Yan et al., Fabrication of diverse CuO nanostructures via hydrothermal method and their photocatalytic properties. J. Mater. Sci. Mater. Electron. **27**(7), 6918–6924 (2016)

5. M. Yang, J. He, X. Hu et al., CuO nanostructures as quartz crystal microbalance sensing layers for detection of trace hydrogen cyanide gas. Environ. Sci. Technol. **45**(14), 6088–6094 (2011)

6. Y. Wang, T. Jiang, D. Meng et al., Fabrication of nanostructured CuO films by electrodeposition and their photocatalytic properties. Appl. Surf. Sci. **317**, 414–421 (2014)

7. D. Shang, Y. Ke, Y. Zhang et al., Magnetic and field emission properties of straw-like CuO nanostructures. Appl. Surf. Sci. **255**(7), 4093–4096 (2009)

8. R.A. Nistor, G.J. Martyna, D.M. Newns et al., Ab initio theory of the pseudogap in cuprate superconductors driven by C4 symmetry breaking. Phys. Rev. B **83**(14), 970–978 (2011)

9. M. Mojahed, S.V. Vaerenbergh, Q. Galand, Nanofluids thermal conductivity measurement in a Bénard cell. Adv. Mech. Eng. **5**, 1–6 (2013)

10. R.V. Kumar, Y. Diamant, A. Gedanken, Sonochemical synthesis and characterization of nanometer-size transition metal oxides from metal acetates. Chem. Mater. **12**(8), 2301–2305 (2000)

11. V. Kumar, S. Masudy-Panah, C.C. Tan et al. Copper oxide based low cost thin film solar cells, in *IEEE*, Nanoelectronics Conference, pp 443–445 (2013)

12. L.J. Zhou, Y.C. Zou, J. Zhao et al., Facile synthesis of highly stable and porous Cu_2O/CuO cubes with enhanced gas sensing properties. Sens. Actuators B **188**, 533–539 (2013)

13. Y. Tian, Y. Liu, W.P. Wang et al., CuO nanoparticles on sulfur-doped graphene for nonenzymatic glucose sensing. Electrochim. Acta **156**, 244–251 (2015)

14. Y. Wang, T. Jiang, D. Meng et al., Synthesis and enhanced photocatalytic property of feather-like Cd-doped CuO nanostructures by hydrothermal method. Appl. Surf. Sci. **355**, 191–196 (2015)

15. N. Liu, Fabrication of smart nanochannels and its application as biosensors. Huazhong University of Science & Technology (2015)

16. K.D. Liang, C.H. Huang, C.C. Lai et al., Single CuO(x) nanowire memristor: forming-free resistive switching behavior. ACS Appl. Mater. Interfaces **6**(19), 16537–16544 (2014)

17. M. Lee, S.C. Hong, D. Kim, Formation of bamboo-like conducting carbon nanotubes decorated with Au nanoparticles by the thermal decomposition of sucrose in an AAO template. Carbon **50**(7), 2465–2471 (2012)

18. J. Kong, T. Zhou, X. Wu et al., Confined assembly of TiO_2, nanostructures in the nanochannels of AAO membrane. J. Mater. Sci. Mater. Electron. **29**(6), 1–7 (2017)

19. T.C. Chan, Y.M. Lin, H.W. Tsai et al., Growth of large-scale nanotwinned Cu nanowire arrays from anodic aluminum oxide membrane by electrochemical deposition process: controllable nanotwin density and growth orientation with enhanced electrical endurance performance. Nanoscale **6**(13), 7332–7338 (2014)

20. D. Han, X. Zhang, Z. Hua et al., A general melt-injection-decomposition route to oriented metal oxide nanowire arrays. Appl. Surf. Sci. **390**, 760–764 (2016)

21. S.U. Yi-Kun, C.M. Shen, H.T. Yang et al., Controlled synthesis of highly ordered CuO nanowire arrays by template-based sol-gel route. Trans. Nonferrous Metals Soc. China **17**(4), 783–786 (2007)

22. A. Kumar, A. Sanger, A. Kumar et al., Highly sensitive and selective CO gas sensor based on a hydrophobic SnO_2/CuO bilayer. RSC Adv **6**(52), 47178–47184 (2016)

23. Z. Sun, F. Zhang, X. Zhang et al., Chiral recognition of Arg based on label-free PET nanochannel. Chem. Commun. **51**(23), 4823–4826 (2015)

24. R. Wang, Y. Sun, F. Zhang et al., Temperature-sensitive artificial channels through pillar[5]arene-based host-guest interactions. Angew. Chem. **129**(19), 5294–5298 (2017)

25. C. Han, X. Hou, H. Zhang et al., Enantioselective recognition in biomimetic single artificial nanochannels. J. Am. Chem. Soc. **133**(20), 7644–7647 (2011)